Reduction of magnetic interlayer coupling in barlowite through isoelectronic substitution

Daniel Guterding,[*] Roser Valentí, and Harald O. Jeschke

Institut für Theoretische Physik, Goethe-Universität Frankfurt, Max-von-Laue-Straße 1, 60438 Frankfurt am Main, Germany

Materials with a perfect kagome lattice structure of magnetic ions are intensively sought after, because they may exhibit exotic ground states like a quantum spin liquid phase. Barlowite is a natural mineral that features perfect kagome layers of copper ions. However, in barlowite there are also copper ions between the kagome layers, which mediate strong interkagome couplings and lead to an ordered ground state. Using *ab initio* density functional theory calculations we investigate whether selective isoelectronic substitution of the interlayer copper ions is feasible. After identifying several promising candidates for substitution we calculate the magnetic exchange couplings based on crystal structures predicted from first-principles calculations. We find that isoelectronic substitution with nonmagnetic ions significantly reduces the interkagome exchange coupling. As a consequence, interlayer-substituted barlowite can be described by a simple two-parameter Heisenberg Hamiltonian, for which a quantum spin liquid ground state has been predicted.

I. INTRODUCTION

The synthesis of herbertsmithite and similar frustrated antiferromagnets with a spin-1/2 kagome lattice has generated in the past intense research efforts because these materials possibly realize a quantum spin liquid (QSL) phase [1–16]. However, a problem in herbertsmithite and related materials is the intrinsic disorder [17–19], which makes the interpretation of experimental data more difficult and might even prevent the formation of a QSL. Therefore, chemical alternatives to herbertsmithite with slightly different bonding environment are intensively sought after [16].

Recently, the geometrically perfect spin-1/2 kagome antiferromagnet barlowite $[Cu_4(OH)_6FBr]$ was discovered [20–23]. It is closely related to herbertsmithite, but shows a different stacking pattern of the kagome layers and features magnetic ions on interplane sites, which couple the kagome planes magnetically and lead to magnetic ordering at low temperatures [22]. Selective doping of nonmagnetic ions into those interplane sites could be a way to remove these interlayer couplings and realize a quantum spin liquid.

Previous calculations showed that substitution with several divalent cations should be possible [23]. These authors predicted that magnesium and zinc can selectively substitute the interlayer copper atoms but did not make a statement about the resulting structure of the magnetic exchange paths. As the interlayer distance in barlowite is relatively small, a finite interlayer exchange can, however, be expected, even when the magnetic ions between the kagome layers are removed.

Using *ab initio* density functional theory (DFT) calculations we investigate the energetics of selectively substituting the copper ions between kagome layers in the barlowite system. In contrast to previous speculations [21] and in agreement with recent calculations [23] we find that isoelectronic doping at the interlayer position becomes energetically less favorable with increasing ionic radius of the substituent. Hence, we

identify ions with a radius similar to Cu^{2+} as the most promising candidates for substitution, such as magnesium or zinc. In this respect we agree with the calculations by Liu *et al.* [23]. We however find that most other ions lead to monoclinically distorted crystal structures with no perfect kagome arrangement of copper ions.

Based on the crystal structures predicted for those substitutions with perfect kagome lattice, we estimate the magnetic exchange couplings in the substituted barlowite system. We find that the corresponding Heisenberg Hamiltonian takes a very simple form with a parameter J_1 describing the nearest-neighbor kagome coupling and a parameter J_2 describing the interlayer exchange energy. We compare our findings to recent model calculations, which suggested a QSL for certain ratios of J_2/J_1 [24].

II. METHODS

Experimental and hypothetical crystal structures were fully relaxed using the projector augmented wave (PAW) method [25] implemented in GPAW [26] with a plane-wave cutoff of 1000 eV and the GGA exchange-correlation functional [27]. We optimized all crystal structures using 4^3 k points until forces were below 10 meV/Å.

We started from the experimental crystal structure of barlowite [20] and substituted the interlayer copper site (Cu^{2+}) by $A =$ Mg^{2+}, Ca^{2+}, Sr^{2+}, Zn^{2+}, Cd^{2+}, Hg^{2+}, Sn^{2+}, Pb^{2+}, forming A-substituted barlowite, $ACu_3(OH)_6FBr$. From this relaxation we obtained the desirable crystal structure with perfect kagome lattice of substituted barlowite in space group $P\,6_3/mmc$, containing two formula units. While most of the cations considered here are almost certainly divalent, tin and lead are more flexible with respect to their oxidation state. Therefore, it has to be verified that these cations indeed assume a divalent state when substituted into barlowite.

From these structures we then constructed related *undesirable* defect structures, where all substituent atoms sit in the kagome plane. After reducing the symmetry to $P\,1$, the unit cell contains three copper atoms for each of two different kagome layers stacked in the z direction. We chose

_____
[*]guterding@itp.uni-frankfurt.de

TABLE I. Calculated isoelectronic doping energies for barlowite. Positive values of the doping energy E_{dop} indicate that the kagome lattice will be distorted upon doping. On the interlayer site, barlowite prefers to incorporate ions with smaller radius than Cu^{2+} (72 pm). Ionic radii in coordination number 6 are taken from Refs. [33,34].

$A =$	Mg^{2+}	Ca^{2+}	Sr^{2+}	Zn^{2+}	Cd^{2+}	Hg^{2+}	Sn^{3+}
E_{dop} (eV)	−0.994	−0.012	0.349	−0.367	0.183	1.282	−0.196
r_{ion} (pm)	72	100	118	74	95	102	81

TABLE II. Predicted structural parameters for Mg-barlowite [$MgCu_3(OH)_6FBr$] ($P6_3/mmc$ space group, $a = 6.79899$ Å, $c = 9.34513$ Å, $Z = 2$).

Atom	Site	x	y	z
Cu	$6g$	$1/2$	0	0
Mg	$2c$	$1/3$	$2/3$	$1/4$
O	$12k$	0.20346	0.40692	0.09419
H	$12k$	0.12545	0.25090	0.13412
Br	$2d$	$1/3$	$2/3$	$3/4$
F	$2b$	0	0	$1/4$

to place one dopant atom in each kagome layer assuming that clustering is not favored. This reduces the number of possible defect configurations to two. Either dopant atoms are stacked in the z direction or placed as far apart as possible, with positioning in the xy plane alternating between the two kagome layers. We decided for the latter case. After full relaxation of these structures with identical chemical composition $ACu_3(OH)_6FBr$, total energies can be compared directly on the DFT level to find whether the substituent ions prefer to occupy the interlayer site or occupy a site in the kagome layer, consequently destroying the perfect kagome lattice.

Total energies and magnetic exchange interactions were evaluated based on the fully relaxed structures using *ab initio* DFT calculations within an all-electron full-potential local orbital (FPLO) [28] basis. For the exchange-correlation functional we employed the generalized gradient approximation (GGA) [27], as well as GGA+U [29] functionals. For the double counting correction we used the fully localized limit. The Hubbard repulsion on the Cu $3d$ orbitals was set to $U = 6$ eV and Hund's rule coupling to $J_H = 1$ eV. This choice of parameters was verified in Ref. [22] by comparing experimental and simulated susceptibility data. For the calculation of magnetic exchange couplings we used a $\sqrt{2} \times \sqrt{2} \times 1$ supercell containing four formula units, i.e.,

twelve inequivalent Cu sites. This allows for 171 unique out of 4096 total spin configurations. The couplings we calculated are based on fits to 25 different spin configurations. For details of the fitting procedure, see Appendix B. As the Cu^{2+} moments are precisely $1\,\mu_B$ and all spin configurations lead to gaps of 1.5 eV for $U = 6$ eV and of 2.2 eV for $U = 8$ eV, fits are very accurate and the resulting statistical error bars tiny. Total energies and Heisenberg models were extracted from calculations converged using 8^3 and 6^3 k-point grids, respectively. Although we found that a sizable Dzyaloshinskii-Moriya interaction is necessary to explain the canted antiferromagnetic state in the original barlowite [22], we do not investigate this parameter here, since it requires calculations beyond the scope of the present study. In studies of the quantum Heisenberg model with Dzyaloshinskii-Moriya interaction, it has been shown that the QSL state we are interested in here is stable with substantial DM values of up to $D \sim 0.1J$ [3,30].

FIG. 1. Calculated isoelectronic doping energies for barlowite. All data points above the zero line indicate that the kagome lattice will be distorted upon doping. On the interlayer site, barlowite prefers to incorporate ions with smaller radius than Cu^{2+} (72 pm). Ionic radii in coordination number 6 are taken from Refs. [33,34].
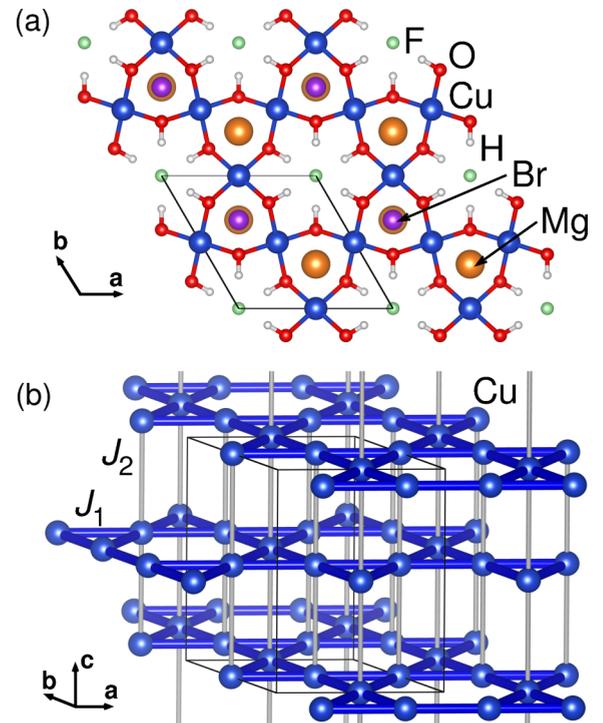
FIG. 2. (a) Crystal structure and (b) magnetic exchange paths in Mg-barlowite, $MgCu_3(OH)_6FBr$.

TABLE III. Predicted structural parameters for Zn-barlowite [$ZnCu_3(OH)_6FBr$] ($P6_3/mmc$ space group, $a = 6.81439$ Å, $c = 9.39923$ Å, $Z = 2$).

Atom	Site	x	y	z
Cu	$6g$	1/2	0	0
Zn	$2c$	1/3	2/3	1/4
O	$12k$	0.20333	0.40666	0.09228
H	$12k$	0.12645	0.25290	0.13526
Br	$2d$	1/3	2/3	3/4
F	$2b$	0	0	1/4

III. RESULTS AND DISCUSSION

The DFT calculated doping energies are given in Table I. Our results show that substitution happens selectively on the interlayer copper site, i.e., structures with perfect kagome layer are obtained only for substitutions of the interlayer Cu^{2+} by magnesium, zinc, and tin. For substitution with calcium the energy difference between doping into the interlayer and into the kagome plane is negligible. For strontium, cadmium, mercury, and lead we find that these substituents prefer to distort the kagome plane. For lead not even a metastable structure with perfect kagome layer could be obtained, therefore no doping energy has been calculated. Surprisingly, we find that tin assumes a configuration Sn^{3+} when substituted into barlowite, which lowers the oxidation state of the Cu^{2+} ions by one third of an electron on average. Consequently the magnetic moments in Sn-barlowite are very fragile, and we did not investigate the magnetic exchange couplings of this system any further. As Sn-barlowite might still be an interesting material, some details on its electronic structure are given in Appendix A.

In Fig. 1 we visualize the doping energy per formula unit of A-substituted barlowite as a function of the ionic radius in coordination number six, taken from Refs. [33,34]. The doping energy is mainly controlled by the ionic radius of the substituents. The chemical details of the substituents only play a minor role, evidenced by the larger absolute doping energy of magnesium compared to zinc or the negative doping energy of calcium compared to a positive doping energy of cadmium, although the latter has a slightly smaller ionic radius.

The doping energies we calculated reproduce the overall trends reported in Ref. [23]. As we performed our calculations directly in the stoichiometric limit, we however found a competing monoclinically distorted crystal structure, which places stronger restrictions on the feasibility of the doping process than the supercell calculations in Ref. [23].

The predicted crystal structure for Mg-barlowite [$MgCu_3(OH)_6FBr$] is given in Table II and visualized in Fig. 2(a). The variant with zinc, Zn-barlowite [$ZnCu_3(OH)_6FBr$], has a very similar structure listed in Table III.

For these optimized crystal structures we calculated the magnetic exchange couplings as described previously. The calculated exchange parameters for Mg-barlowite and Zn-barlowite are listed in Table IV. The coupling constants are sorted so that the index increases with the Cu-Cu distance along the bond. Couplings J_1, J_4, and J_5 connect to the first, second, and third neighbors within the kagome plane, while J_2, J_3, J_6, and J_7 are interlayer couplings with a Cu-Cu distance of up to 8.3 Å. We find that only the exchange parameters J_1 and J_2 are relevant. The corresponding paths are visualized in Fig. 2(b). The resulting spin-1/2 Heisenberg Hamiltonian therefore contains antiferromagnetic couplings J_1 along the nearest-neighbor bonds in the kagome plane, indicated by symbol $\langle i, j \rangle$, and antiferromagnetic couplings J_2 along bonds perpendicular to the kagome layer, indicated by symbol $[i, j]$:

$$H = J_1 \sum_{\langle i,j \rangle} \vec{S}_i \cdot \vec{S}_j + J_2 \sum_{[i,j]} \vec{S}_i \cdot \vec{S}_j.$$

In the sums, each bond is only counted once. The exchange parameters in Zn-barlowite are somewhat larger than in Mg-barlowite. The larger J_1 in Zn-barlowite may be a consequence of the Cu-O-Cu bond angles of 117.8° (Zn-barlowite) versus 117.2° (Mg-barlowite). The antiferromagnetic contribution to the superexchange is enhanced when the bond angle gets closer to 180°. The same evolution of exchange interactions with bond angle is observed in the similar compounds herbertsmithite, kapellasite, and haydeeite [14], $(Zn,Mg,Cd)Cu_3(OH)_6Cl_2$. The slightly larger J_2 in Zn-barlowite could be related to the larger ionic radius of Zn^{2+} compared to Mg^{2+}, which could enhance the exchange interaction. Taking into account the statistical errors listed in Table IV, the difference is however very small.

For the original barlowite system we estimated Heisenberg couplings $J_{b1} = 177$ K for next-neighbor exchange within the kagome plane and $J_{b2} = -205$ K between spins within the kagome plane and interlayer copper spins [22]. The strong interlayer coupling is clearly removed upon substitution, and the intralayer coupling retains the same order of magnitude. With $U = 6$ eV we estimate a ratio of $J_2/J_1 = 0.06$ for Mg-barlowite and $J_2/J_1 = 0.07$ for Zn-barlowite. A QSL has recently been predicted [24] for this J_1-J_2 model in the range $|J_2/J_1| < 0.15$. Thus, we predict the two barlowite variants

TABLE IV. Calculated exchange couplings for the theoretically predicted Mg-barlowite, $MgCu_3(OH)_6FBr$, and Zn-barlowite, $ZnCu_3(OH)_6FBr$. A GGA+U functional with $J_H = 1$ eV and the two listed U values were used in combination with a fully localized limit double counting correction [31,32]. Antiferromagnetic couplings are positive, while ferromagnetic couplings are negative. The statistical errors of the exchange parameters from the fitting procedure are given in brackets.

$A=$	U (eV)	J_1 (K)	J_2 (K)	J_3 (K)	J_4 (K)	J_5 (K)	J_6 (K)	J_7 (K)	J_2/J_1
Mg^{2+}	6.0	226(1)	13.4(6)	0.0(4)	1.1(4)	−1.0(4)	0.1(3)	−0.4(2)	0.06
	8.0	167(1)	10.0(4)	0.1(2)	0.4(3)	−0.8(2)	0.0(2)	−0.2(1)	0.06
Zn^{2+}	6.0	240(1)	15.4(5)	0.8(2)	0.8(3)	−1.0(2)	−0.7(2)	−0.7(2)	0.07
	8.0	179(1)	11.0(3)	0.5(2)	0.1(2)	−0.9(2)	−0.4(2)	−0.4(1)	0.07

TABLE V. Predicted structural parameters for Sn-barlowite [SnCu$_3$(OH)$_6$FBr] ($P\,6_3/mmc$ space group, $a = 6.73194$ Å, $c = 9.99153$ Å, $Z = 2$).

Atom	Site	x	y	z
Cu	6g	$^1\!/_2$	0	0
Sn	2c	$^1\!/_3$	$^2\!/_3$	$^1\!/_4$
O	12k	0.20061	0.40122	0.10735
H	12k	0.12368	0.24736	0.14979
Br	2d	$^1\!/_3$	$^2\!/_3$	$^3\!/_4$
F	2b	0	0	$^1\!/_4$

Mg-barlowite and Zn-barlowite to be not only stable materials, but also very promising spin liquid candidates.

IV. SUMMARY

In summary, we performed *ab initio* density functional theory calculations for isoelectronically substituted barlowite. We showed that only magnesium and zinc can be expected to selectively substitute the interlayer copper atoms in barlowite. Based on the *ab initio* relaxed structures for Mg-barlowite and Zn-barlowite we predicted that these systems are accurately described by a two-parameter Heisenberg model including the nearest-neighbor kagome exchange and the exchange perpendicular to the kagome layers. According to our calculations both Mg-barlowite and Zn-barlowite lie in the region of model parameters for which a quantum spin liquid ground
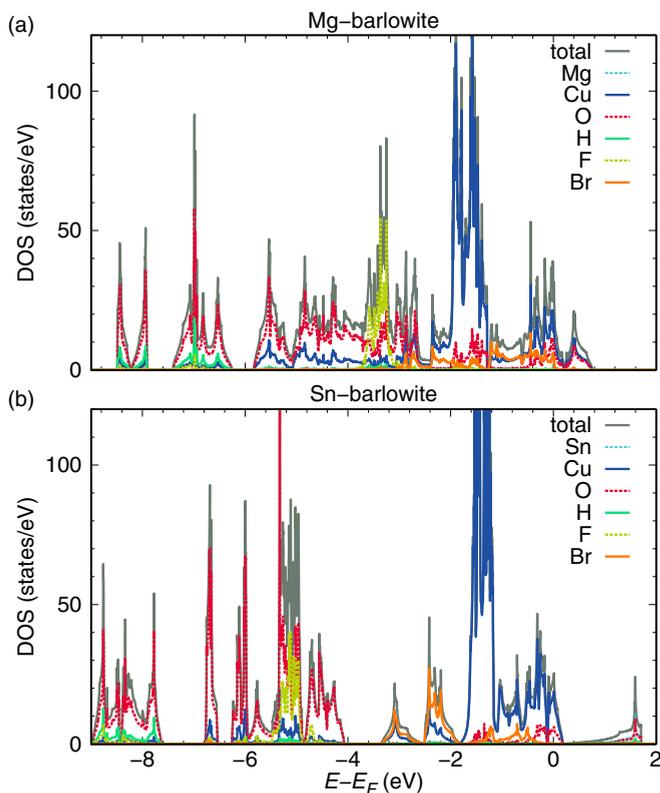
state has recently been predicted. Therefore, we expect that the synthesis of either of these substituted barlowite systems will provide an alternative to the established herbertsmithite system.

APPENDIX A: ELECTRONIC STRUCTURE OF Sn-BARLOWITE IN COMPARISON TO Mg-BARLOWITE

The predicted crystal structure for Sn-barlowite is listed in Table V. Compared to the compounds with the smaller magnesium and tin ions (see Tables II and III) the a axis is somewhat contracted, while the c axis is significantly larger. The difference in the c axes of Mg-barlowite and Zn-barlowite can be directly explained from the different size of Mg^{2+} and Zn^{2+} ions. In Sn-barlowite the c-axis expansion is much larger than the difference in ionic radius. Therefore, the expansion mechanism must be more involved.

The calculated GGA density of states for Mg-barlowite and Sn-barlowite is shown in Fig. 3. The most prominent difference

FIG. 3. Calculated GGA density of states for (a) Mg-barlowite and (b) Sn-barlowite.
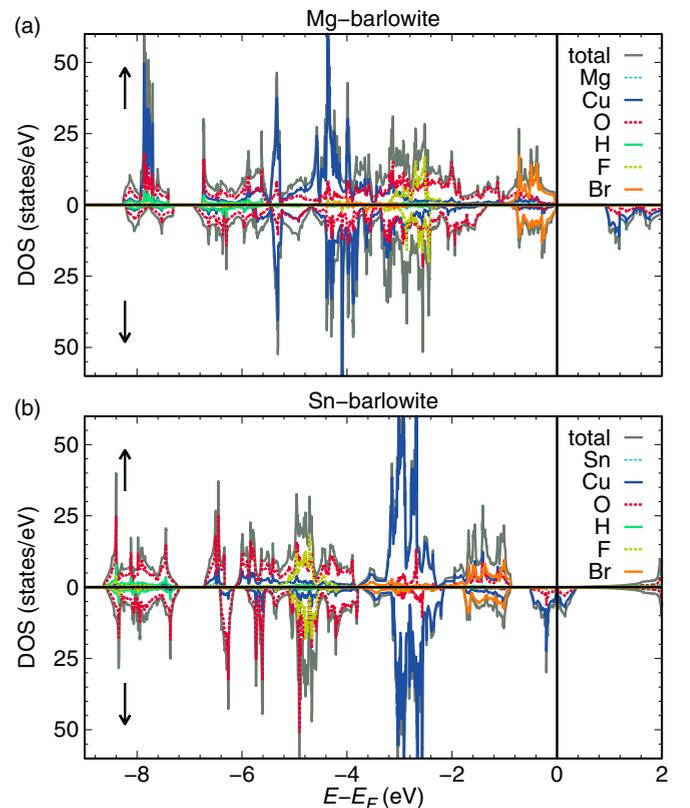
FIG. 4. Calculated spin-resolved GGA+U ($U = 6$ eV, $J_H = 1$ eV) density of states for (a) Mg-barlowite and (b) Sn-barlowite in the ferromagnetic state. The top panel of each subplot shows the DOS of the minority spin channel, while the bottom panel shows the DOS of the majority spin channel.
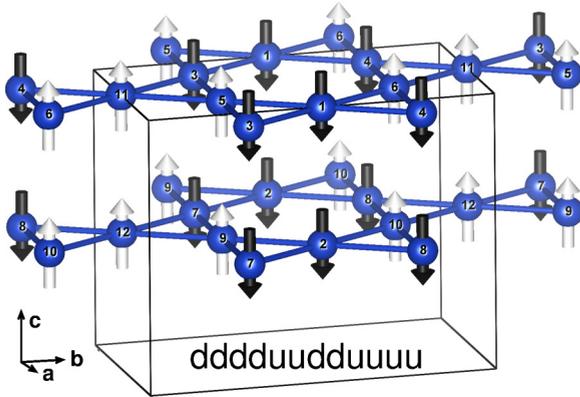
FIG. 5. Example for the spin configurations used in the energy mapping. Only the Cu^{2+} ion positions for a $\sqrt{2} \times \sqrt{2} \times 1$ supercell of Zn-barlowite are shown. The numbers on the twelve inequivalent Cu^{2+} ions allow encoding of the spin configuration indicated with arrows as the string "dddduuddduuuu" where d $\equiv\downarrow$ and u $\equiv\uparrow$.

between the two materials is the distribution of the bromine and fluorine states, which are shifted to much lower energies in Sn-barlowite. Especially the hybridization between bromine and copper is very much reduced.

Furthermore, integration of the copper density of states reveals that the occupation is one electron higher than in Mg-barlowite, while tin is in a trivalent state. We conclude that tin donates an additional electron into the copper kagome layer. This behavior can be rationalized based on the observation that doping onto the interlayer site becomes more stable with smaller ionic radius (see Fig. 1). While Sn^{2+} has an ionic radius of 93 pm [35], Sn^{3+} has an ionic radius of 81 pm. As a consequence Sn-barlowite can gain energy by reducing the ionic radius as tin becomes trivalent.

The strong expansion of the c axis can be explained by an elongation of the Cu-O bonds due to the additional charge on the copper atoms donated from tin. This reduction of Cu-O hybridization is directly visible in the density of states (see Fig. 3). This in turn might explain the large shift in bromine and fluorine energy levels compared to Mg-barlowite. Elongation of Cu-O bonds induces a shrinking of the F-H bonds, which leads to a strong lowering of the fluorine energy levels. Bromine on the other hand almost exclusively hybridizes with copper, and these Cu-Br bonds are significantly elongated in Sn-barlowite, probably again due to the additional charge available on the copper atoms. Therefore, the hybridization between bromine and copper is reduced and bromine states are less relevant in the vicinity of the Fermi level.
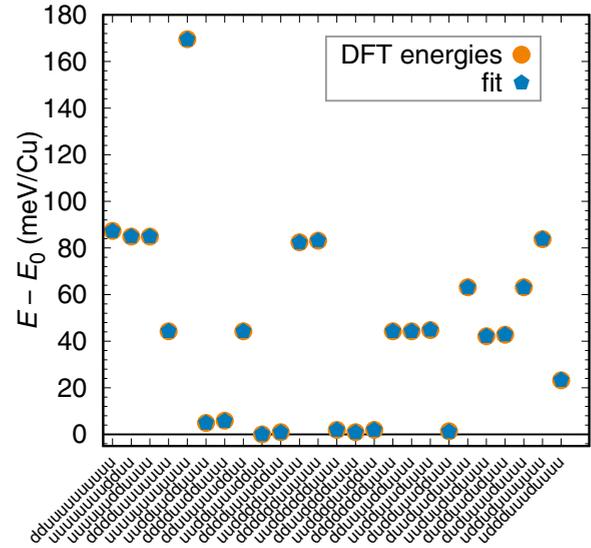
FIG. 6. Comparison between calculated total energies per Cu^{2+} ion for 25 different spin configurations in a $\sqrt{2} \times \sqrt{2} \times 1$ supercell of Zn-barlowite and classical energies of a Heisenberg Hamiltonian with J_1 to J_7 as given in Table IV ($U = 6$ eV line).

Additionally, we show in Fig. 4 the spin-resolved GGA+U density of states for ferromagnetic arrangement of copper moments. In our calculations, Mg-barlowite clearly becomes insulating once magnetism and interactions are considered, while Sn-barlowite stays metallic due to to the additional electron in the copper kagome layer, leading to 4/3 filling [13].

APPENDIX B: CALCULATION OF HEISENBERG EXCHANGE COUPLINGS BY MAPPING OF DFT ENERGIES

Figures 5 and 6 illustrate the energy mapping method used to extract Heisenberg Hamiltonian parameters from DFT total energies. Energy mapping is a widely used standard method in the context of spin systems [5,22,36–39].

All 4096 spin configurations for the twelve inequivalent Cu spins of a $\sqrt{2} \times \sqrt{2} \times 1$ supercell of doped barlowite with P 1 symmetry are classified with respect to their classical exchange energy. Representatives for the 25 distinct energy values are chosen (one example is shown in Fig. 5), and total DFT energies are calculated (filled circles in Fig. 6). Fitting these energies to classical exchange energies yields the seven exchange couplings shown in the third line of Table IV, with small statistical errors. The quality of the fit is illustrated by the classical exchange energies, shown in Fig. 6 as pentagons.

[1] M. P. Shores, E. A. Nytko, B. M. Bartlett, and D. G. Nocera, A Structurally Perfect $S = 1/2$ Kagomé Antiferromagnet, J. Am. Chem. Soc. **127**, 13462 (2005).

[2] P. Mendels and F. Bert, Quantum kagome antiferromagnet ZnCu3(OH)6Cl2, J. Phys. Soc. Jpn. **79**, 011001 (2010).

[3] P. Mendels and F. Bert, Quantum kagome antiferromagnet: ZnCu3(OH)6Cl2, J. Phys. Conf. Ser. **320**, 012004 (2011).

[4] R. H. Colman, A. Sinclair, and A. S. Willis, Comparisons between Haydeeite, α-Cu3Mg(OD)6Cl2, and Kapellasite, α-Cu3Zn(OD)6Cl2, Isostructural $S = 1/2$ kagome magnets, Chem. Mater. **22**, 5774 (2010).

[5] H. O. Jeschke, F. Salvat-Pujol, and R. Valentí, First-principles determination of Heisenberg Hamiltonian parameters for the spin-1/2 kagome antiferromagnet ZnCu3(OH)6Cl2, Phys. Rev. B **88**, 075106 (2013).

[6] Y. Li, B. Pan, S. Li, W. Tong, L. Ling, Z. Yang, J. Wang, Z. Chen, Z. Wu, and Q. Zhang, Gapless quantum spin liquid in the $S = 1/2$ anisotropic kagome antiferromagnet $ZnCu_3(OH)_6SO_4$, New J. Phys. **16**, 093011 (2014).

[7] Y. Li and Q. Zhang, Structure and magnetism of $S = 1/2$ kagome antiferromagnets $NiCu_3(OH)_6Cl_2$ and $CoCu_3(OH)_6Cl_2$, J. Phys.: Condens. Matter **25**, 026003 (2013).

[8] T.-H. Han, J. S. Helton, S. Chu, D. G. Nocera, J. A. Rodriguez-Rivera, C. Broholm, and Y. S. Lee, Fractionalized excitations in the spin-liquid state of a kagome-lattice antiferromagnet, Nature (London) **492**, 406 (2012).

[9] R. H. Colman, A. Sinclair, and A. S. Wills, Magnetic and crystallographic studies of Mg-Herbertsmithite, γ-$Cu_3Mg(OH)_6Cl_2$ – A new $S = 1/2$ kagome magnet and candidate spin liquid, Chem. Mater. **23**, 1811 (2011).

[10] S. Yan, D. A. Huse, and S. R. White, Spin-liquid ground state of the $S = 1/2$ kagome Heisenberg antiferromagnet, Science **332**, 1173 (2011).

[11] B. Bauer, L. Cincio, B. P. Keller, M. Dolfi, G. Vidal, S. Trebst, and A. W. W. Ludwig, Chiral spin liquid and emergent anyons in a Kagome lattice Mott insulator, Nat. Commun. **5**, 5137 (2014).

[12] Y.-C. He, D. N. Sheng, and Y. Chen, Obtaining topological degenerate ground states by the density matrix renormalization group, Phys. Rev. B **89**, 075110 (2014).

[13] I. I. Mazin, H. O. Jeschke, F. Lechermann, H. Lee, M. Fink, R. Thomale, and R. Valentí, Theoretical prediction of a strongly correlated Dirac metal, Nat. Commun. **5**, 4261 (2014).

[14] Y. Iqbal, H. O. Jeschke, J. Reuter, R. Valentí, I. I. Mazin, M. Greiter, and R. Thomale, Paramagnetism in the kagome compounds $(Zn, Mg, Cd)Cu_3(OH)_6Cl_2$, Phys. Rev. B **92**, 220404(R) (2015).

[15] D. Guterding, H. O. Jeschke, and R. Valentí, Prospect of quantum anomalous Hall and quantum spin Hall effect in doped kagome lattice Mott insulators, Sci. Rep. **6**, 25988 (2016).

[16] M. R. Norman, Herbertsmithite and the search for the quantum spin liquid, arXiv:1604.03048.

[17] S.-H. Lee, H. Kikuchi, Y. Qiu, B. Lake, Q. Huang, K. Habicht, and K. Kiefer, Quantum-spin-liquid states in the two-dimensional kagome antiferromagnets $Zn_xCu_{4-x}(OD)_6Cl_2$, Nat. Mater. **6**, 853 (2007).

[18] M. A. de Vries, K. V. Kamenev, W. A. Kockelmann, J. Sanchez-Benitez, and A. Harrison, Magnetic Ground State of an Experimental $S = 1/2$ Kagome Antiferromagnet, Phys. Rev. Lett. **100**, 157205 (2008).

[19] D. E. Freedman, T. H. Han, A. Prodi, P. Müller, Q.-Z. Huang, Y.-S. Chen, S. M. Webb, Y. S. Lee, T. M. McQueen, and D. G. Nocera, Site specific x-ray anomalous dispersion of the geometrically frustrated kagomé magnet, Herbertsmithite $ZnCu_3(OH)_6Cl_2$, J. Am. Chem. Soc **132**, 16185 (2010).

[20] P. Elliott and M. A. Cooper, Barlowite, $Cu_4FBr(OH)_6$, a new mineral isotructural with claringbullite: Description and crystal structure, Mineralog. Mag. **78**, 1755 (2014).

[21] T.-H. Han, J. Singleton, and J. A. Schlueter, Barlowite: A Spin-1/2 Antiferromagnet with a Geometrically Perfect Kagome Motif, Phys. Rev. Lett. **113**, 227203 (2014).

[22] H. O. Jeschke, F. Salvat-Pujol, E. Gati, N. H. Hoang, B. Wolf, M. Lang, J. A. Schlueter, and R. Valentí, Barlowite as a canted antiferromagnet: Theory and experiment, Phys. Rev. B **92**, 094417 (2015).

[23] Z. Liu, X. Zou, J.-W. Mei, and F. Liu, Selectively doping barlowite for quantum spin liquid: A first-principles study, Phys. Rev. B **92**, 220102(R) (2015).

[24] O. Götze and J. Richter, The route to magnetic order in the spin-1/2 kagome Heisenberg antiferromagnet: The role of interlayer coupling, Europhys. Lett. (EPL) **114**, 67004 (2016).

[25] P. E. Blöchl, Projector augmented-wave method, Phys. Rev. B **50**, 17953 (1994).

[26] J. Enkovaara, C. Rostgaard, J. J. Mortensen, J. Chen, M. Dułak, L. Ferrighi *et al.*, Electronic structure calculations with GPAW: a real-space implementation of the projector augmented-wave method, J. Phys.: Condens. Matter **22**, 253202 (2010).

[27] J. P. Perdew, K. Burke, and M. Ernzerhof, Generalized Gradient Approximation Made Simple, Phys. Rev. Lett. **77**, 3865 (1996).

[28] K. Koepernik and H. Eschrig, Full-potential nonorthogonal local-orbital minimum-basis band-structure scheme, Phys. Rev. B **59**, 1743 (1999).

[29] A. I. Liechtenstein, V. I. Anisimov, and J. Zaanen, Density-functional theory and strong interactions: Orbital ordering in Mott-Hubbard insulators, Phys. Rev. B **52**, R5467(R) (1995).

[30] L. Messio, O. Cépas, and C. Lhuillier, Schwinger-boson approach to the kagome antiferromagnet with Dzyaloshinskii-Moriya interactions: Phase diagram and dynamical structure factors, Phys. Rev. B **81**, 064428 (2010).

[31] V. I. Anisimov, I. V. Solovyev, M. A. Korotin, M. T. Czyzyk, and G. A. Sawatzky, Density-functional theory and NiO photoemission spectra, Phys. Rev. B **48**, 16929 (1993).

[32] S. L. Dudarev, G. A. Botton, S. Y. Savrasov, C. J. Humphreys, and A. P. Sutton, Electron-energy-loss spectra and the structural stability of nickel oxide: An LSDA+U study, Phys. Rev. B **57**, 1505 (1998).

[33] R. D. Shannon, Revised effective ionic radii and systematic studies of interatomic dinstances in halides and chalcogenides, Acta Cryst. A **32**, 751 (1976).

[34] H. Yanagida, K. Kōmoto, and M. Miyayama, *The Chemistry of Ceramics* (John Wiley & Sons, Chichester, 1996).

[35] H. Djieutedjeu, X. Zhou, H. Chi, N. Haldolaarachchige, K. G. S Ranmohotti, C. Uher, D. Young, and F. P. Poudeu, Donor and acceptor impurity-driven switching of magnetic ordering in $MnSb_{2-x}Sn_xSe_4$, J. Mater. Chem. C **2**, 6199 (2014).

[36] H. Rosner, R. R. P. Singh, W. H. Zheng, J. Oitmaa, S.-L. Drechsler, and W. E. Pickett, Realization of a Large J_2 Quasi-2D Spin-Half Heisenberg System: Li_2VOSiO_4, Phys. Rev. Lett. **88**, 186405 (2002).

[37] S.-L. Drechsler, O. Volkova, A. N. Vasiliev, N. Tristan, J. Richter, M. Schmitt, H. Rosner, J. Málek, R. Klingeler, A. A. Zvyagin, and B. Büchner, Frustrated Cuprate Route from Antiferromagnetic to Ferromagnetic Spin-$\frac{1}{2}$ Heisenberg Chains: Li_2ZrCuO_4 as a Missing Link near the Quantum Critical Point, Phys. Rev. Lett. **98**, 077202 (2007).

[38] H. O. Jeschke, I. Opahle, H. Kandpal, R. Valentí, H. Das, T. Saha-Dasgupta *et al.*, Multi-Step Approach to Microscopic Models for Frustrated Quantum Magnets: The Case of the Natural Mineral Azurite, Phys. Rev. Lett. **106**, 217201 (2011).

[39] J. K. Glasbrenner, I. I. Mazin, H. O. Jeschke, P. J. Hirschfeld, R. M. Fernandes, and R. Valentí, Effect of magnetic frustration on nematicity and superconductivity in Fe chalcogenides, Nat. Phys. **11**, 953 (2015).